Characterization of the Point Spread Function for the x-ray pinhole cameras at ALBA Synchrotron

Author: Ingrid Mases Solé and Advisor: Antoni García-Santiago
*Facultat de Física, Universitat de Barcelona, Diagonal 645, 08028 Barcelona, Catalonia, Spain.**

Advisor: Ubaldo Iriso Áriz
Sincrotró Alba, Carrer de la Llum 2, 08290 Cerdanyola del Vallès, Catalonia, Spain.

Abstract: The ALBA facility is a Synchrotron Light Source that accelerates electrons up to 3 GeV to produce synchrotron radiation for scientific experiments. Transverse size measurements of the electron beam are carried out by imaging with an x-ray pinhole camera, whose spatial resolution is described by the Point Spread Function (PSF). The PSF changes slightly the beam image and determines the minimum beam size measurable, therefore its value is required for precise beam size measurements. This report calculates and compares the PSF analytically, experimentally and by numerical simulations, showing that the results obtained by the three methods are consistent. ALBA is equipped with a pinhole since 2011, and a new one is under design with a better resolution. Finally, this report also calculates the heat load received at the main pinhole elements to evaluate the need of cooling systems.

I. INTRODUCTION

The ALBA Synchrotron Light Source is a high energy electron accelerator located in Cerdanyola del Vallès (Barcelona). The ALBA facility comprises an injection system, which delivers electrons to a storage ring of 268 m circumference to produce the synchrotron radiation that the beamlines (experimental stations) use to perform research in many different fields, from nanotechnology to biology. Currently, there are 8 beamlines in operation, which receive the x-rays produced when the electron beam is curved by the magnetic structures in the storage ring.

Measuring the transverse size and emittance [1] of the electron beam at any time is essential to control the machine performance, and it is carried out with an x-ray pinhole camera [2]. The pinhole image is affected by the system Point Spread Function (PSF) which is the beam size measured at the screen camera corresponding to a point-like electron beam, also called "zero emittance beam". Characterization of the pinhole PSF allows to accurately calculate the transverse beam size.

Currently, one x-ray pinhole is operating at ALBA and it is located at the Front End 34 (FE34). For redundancy purposes, another one is currently under design at FE21.

In this paper, the PSF is calculated by three different methods: analytically, experimentally and by numerical simulations using a program called OASYS which is a graphical interface for performing optical simulations and beamline configurations [3]. Until now, the PSF has only been calculated analytically for pinhole in FE34 [4]. Now that another pinhole is being designed, we aim to compare the analytical calculations with the experimental results and simulations. The work is the result of a four months stay I performed at ALBA from October 2019 to January 2020.

*Electronic address: imasesso7@alumnes.ub.edu

II. THE ALBA X-RAY PINHOLE

The ALBA x-ray pinhole is a beam diagnostics system used to measure the electron beam size in the storage ring, as well as beam position and stability. As the simple optics principle of a pinhole (Fig.1 - top), it takes the synchrotron radiation coming from a bending magnet to obtain a magnified transverse image of the electron beam, which will be analysed to infer the vertical and horizontal electron beam size.

The main parameters of the electron beam and the dipole bending magnet are summarized in Table I.

Horizontal electron beam size σ_x	58 μm
Vertical electron beam size σ_y	26 μm
Horizontal electron beam divergence $\sigma_x^{'}$	33 μrad
Vertical electron beam divergence $\sigma_y^{'}$	26 μrad
Energy, E	3 GeV
Energy spread , $\frac{\triangle E}{E}$	0.001
Number of bunches (max)	448
Current intensity, I	250 mA
Dipole magnet field, B	1.42 T
Lorentz relativistic factor, γ	5870

Table I: ALBA electron beam and dipole parameters. They are used as input for OASYS. σ_x and σ_y are Gaussian standard deviations.

A. Experimental set-up

The sketch of the x-ray pinhole located at FE34 is shown in Fig.1 (bottom). The pinhole consists of the following elements. First, a fixed mask limits the radiation aperture: 1 mrad horizontally and 0.5 mrad vertically. Next, the Aluminium window with a thickness of 1 mm separates the vacuum region and air at atmospheric pressure, and it also filters out the softest x-rays. The next element is a triangular prism Cu filter whose thickness can be adjusted to select the hard x-rays. The radiation then goes through the pinhole of aperture w made of Tungsten. The last component is a YAG (Yttrium Aluminium Garnet) fluorescence screen that converts x-rays

into visible light which is finally imaged through a lens system on a CCD.

Naming L_1 the distance from the source point to the pinhole and L_2 the distance between the pinhole and the YAG screen, the image of an electron beam with transverse size σ_b is amplified as $\frac{L_2}{L_1}\sigma_b$. The subindex b stands for both the horizontal, x, and vertical, y, sizes. Note that the image on the screen is slightly modified by blurring and diffraction effects, as explained in the next section.

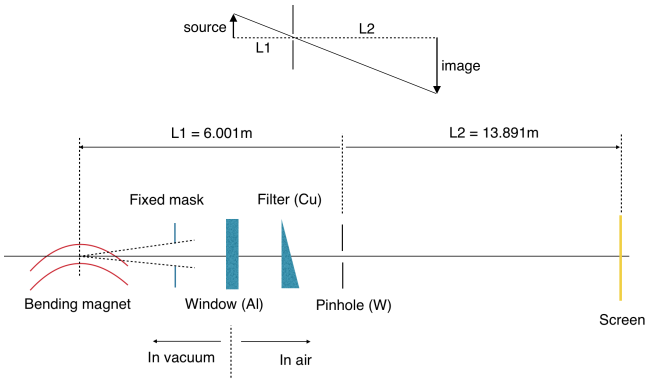

Figure 1: Working principle of a pinhole (top). Component schematics of FE34 pinhole system (bottom). Dimensions are not to scale.

A new pinhole is being designed at Front End 21 (FE21), with some improvements with respect to the pinhole at FE34. The main parameter difference is the magnification, which increases from 2.31 to 3.76. Table II lists the main parameters of both pinholes.

	Pinhole FE34	Pinhole FE21
L_1 (m)	6.001	4.152
L_2 (m)	13.891	15.624
Magnification $X = L_2/L_1$	2.31	3.76
Al window width (mm)	1	1.5

Table II: Values for L_1, L_2, magnification and thickness of the Aluminium window for both pinholes.

B. OASYS Simulations

OASYS is a Python based program and, among others, it includes the codes SHADOW (for ray tracing simulations) and SRW (for synchrotron radiation wavefront propagation). Configurations of both pinholes are simulated with OASYS. On the one hand, SHADOW is used to simulate the magnified image of the electron beam to calculate the beam size. On the other hand, SRW is used to compute the pinhole PSF.

Two examples of the transverse beam image acquired with SHADOW simulations of pinhole FE34 and FE21 are shown in Fig. 2. Vertical and horizontal projections follow Gaussian profiles, and so we obtain σ_x and σ_y using 2D Gaussian fits. The image obtained with the pinhole at FE21 shows larger dimensions than the image obtained with pinhole at FE34 because of larger magnification in FE21.

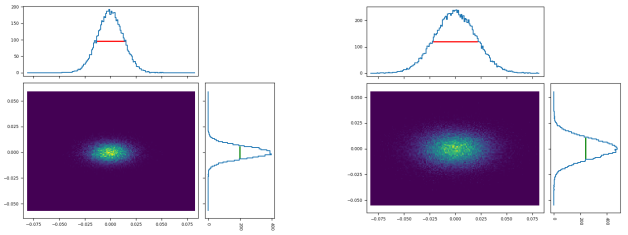

(a) FE34 (b) FE21

Figure 2: Comparison of beam images in both pinholes systems, simulated with OASYS.

OASYS is also used to calculate the photon flux produced by a bending dipole, and it also allows to see how this flux evolves after traversing different thickness of Al and Cu – see Fig. 3. Note that the flux is not monochromatic, which influences the calculation of the PSF (see next Section).

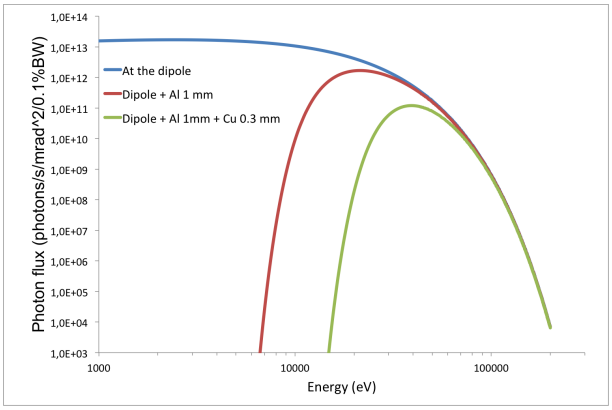

Figure 3: Radiation spectrum produced by a bending dipole of ALBA (blue), radiation attenuated by an Al window of 1 mm (red), and radiation attenuated by an Al window of 1 mm + Cu filter of 0.3 mm (green). Data obtained with OASYS.

III. CALCULATION OF PSF

The PSF can be calculated using different methods. First, the analytical method is used to show the different effects contributing to the beam size enlargement. Next, OASYS simulations are performed. Finally, an experimental method using the measurement of the beam lifetime is carried out to infer the PSF at FE34.

A. Theoretical Analysis

The visible range of synchrotron light is not appropriate for imaging due to diffraction limitation. Instead, the x-ray part of the spectrum is used. This part is affected by Fraunhofer diffraction [4, 5],

$$\sigma_{\text{diff}} = \frac{\sqrt{12}}{4\pi}\frac{\lambda L_2}{w}, \tag{1}$$

and by blurring due to the finite size of the pinhole [4, 5],

$$\sigma_{\text{blur}} = \frac{w(L_1 + L_2)}{\sqrt{12}L_1}, \tag{2}$$

where λ is the wavelength of light and w is the pinhole width. As seen in Fig. 3, the photon beam is not monochromatic and the diffraction contribution must be calculated integrating for the different energies, E. Taking into account that $E = h\frac{c}{\lambda}$,

$$\sigma_{\mathrm{DIFF}} = \int \sigma_{\mathrm{diff}}(E)P(E)\,dE, \tag{3}$$

where

$$P(E) = \frac{N_{\mathrm{ph}}(E)}{\int_0^\infty N_{\mathrm{ph}}(E)\,dE}. \tag{4}$$

Here $N_{\mathrm{ph}}(E)$ is the photon flux for a specific energy.

Then, the PSF is obtained by adding these contributions in quadrature:

$$\sigma_{\mathrm{PSF}} = \sqrt{\sigma_{\mathrm{blur}}^2 + \sigma_{\mathrm{DIFF}}^2 + \sigma_{\mathrm{screen}}^2}, \tag{5}$$

where σ_{screen} is the CCD pixel size. For the electron beam, the measured beam size σ_{YAG} will be larger than the true beam size, $X\sigma_{\mathrm{b}}$, due to its PSF

$$\sigma_{\mathrm{YAG}}^2 = (X\sigma_{\mathrm{b}})^2 + (\sigma_{\mathrm{PSF}})^2, \tag{6}$$

where X is the magnification of the pinhole.

Table III summarises the values of σ_{blur}, σ_{DIFF} and σ_{PSF} for both pinholes, with and without 0.3 mm of Cu for a pinhole width of 10 μm. This value was chosen at FE34 for manufacturing purposes and because it is close to the value that minimizes the σ_{PSF} [4].

	FE34 1mm Al+0.3mm Cu	FE21 1.5mm Al+0.3mm Cu
σ_{blur}	9.57 μm	13.75 μm
σ_{DIFF}	11.2 μm	12.5 μm
σ_{PSF}	**15.19 μm**	**18.93 μm**
	FE34 1mm Al	FE21 1.5mm Al
σ_{blur}	9.57 μm	13.75 μm
σ_{DIFF}	19.2 μm	19.8 μm
σ_{PSF}	**21.76 μm**	**24.40 μm**

Table III: Values of PSF for both pinholes. The value of σ_{screen} is 3.75 μm, corresponding to the CCD pixel size.

The values of σ_{PSF} obtained for the pinhole in FE21 are larger than the ones of pinhole in FE34 because the magnification of pinhole FE21 is larger. Despite this fact, the resolution (in terms of minimum measurable beam size) of FE21 pinhole is better than FE34. Note that $\frac{\sigma_{\mathrm{PSF}}}{X}$ is the minimum beam size a pinhole can measure. Then, the resolution of the pinholes are 6.58 μm (FE34) and 5.03 μm (FE21), in the case with Cu filter of 0.3mm.

Also note that the effect of adding in quadrature the σ_{PSF} in Eq. (6) to the vertical beam size $\sigma_{\mathrm{y}} \sim 30$ μm is not remarkable in the Cu filter case, because

$$\sqrt{\frac{(X\sigma_{\mathrm{y}})^2}{(X\sigma_{\mathrm{y}})^2 + (\sigma_{\mathrm{PSF}})^2}} = \begin{cases} 96.9\%, & \text{FE34} \\ 98.2\%, & \text{FE21.} \end{cases} \tag{7}$$

The effect of σ_{PSF} on the horizontal beam size of the image, $X\sigma_{\mathrm{x}}$, is even smaller because $\sigma_{\mathrm{x}} \sim 2{\cdot}\sigma_{\mathrm{y}}$ (see Table I). In general, note that the relative effect of the PSF contribution to the measured beam size σ_{YAG} reduces as the beam size increases.

B. PSF Calculation using SRW

SRW (Synchrotron Radiation Workshop) is a wave optics computer simulation code integrated in OASYS, and it simulates the radiation wavefront propagation through the elements of an x-ray beamline. We use it to calculate the PSF of pinholes at FE34 and FE21.

For these simulations we consider the wavefront of light emitted by a point-like ("zero emittance") beam. We perform the simulations using a 10 μm horizontal and 1 μm vertical, which is a factor ~ 30 smaller than the real vertical σ_{y} and it is a good compromise between an optimum simulation result and the CPU time. The σ_{PSF} is computed in the vertical plane, which corresponds to the more restringent case.

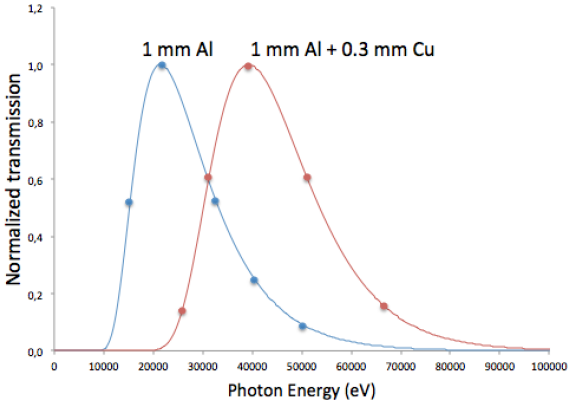

Figure 4: Normalized transmission spectra for 1 mm Al (blue) versus 1 mm Al + 0.3 mm Cu (red) filters at FE34.

The radiation spectrum considering 1 mm Al window and 1 mm Al + 0.3 mm Cu filter are used for pinhole FE34 simulations. On the other hand, the radiation spectrum after 1.5 mm Al window and after 1.5 mm Al window + 0.3 mm Cu filter are used for pinhole FE21 simulations. Since SRW only allows doing simulations with a monochromatic photon flux, several simulations are done with different values of energy to overcome this issue (see Fig. 5, top). Then, we weight the PSF result obtained for each energy according to its normalized flux (see Fig. 4), and we add these contributions in one single profile (red dots in Fig. 5, bottom). The σ_{PSF} is obtained after fitting the profile in Fig. 5 (bottom) to a Gaussian function.

Table IV summarises the values of σ_{PSF} obtained for both pinholes, with and without Copper filter. We stress that the effect of adding the Copper filter is significant because it reduces the value of σ_{PSF} by about 20%.

	FE34	FE21
Al+0.3mm Cu	**14.84 μm**	**18.87 μm**
Al	**17.86 μm**	**23.31 μm**

Table IV: σ_{PSF} values for both pinholes, with and without Cu filter.

In this situation, the minimum beam size measurable are 6.42 μm (in FE34) and 5.02 μm (FE21), in the case with Cu filter.

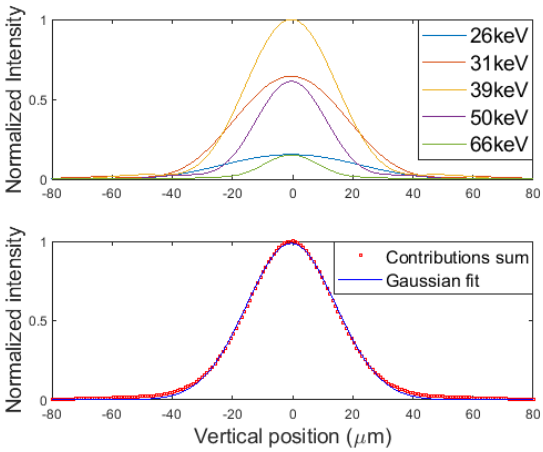

Figure 5: FE34 PSF obtained at the screen for five different energies (top). A Copper filter of 0.3 mm is used. Sum of all PSF contributions (bottom).

C. Experimental Measurement of PSF

The beam lifetime is the time interval after which the intensity of the beam has reached $\frac{1}{e}$ of its initial value. It is given by several effects (vacuum pressure, beam intensity, etc), but the most influencing one is the Touschek effect.

The Touschek effect is a phenomenon of scattering and loss of electrons in the stored electron beam, caused by Coulomb scattering. It consists in the transformation of a small transverse momentum into a large longitudinal momentum [6]. Consequently, both colliding particles are lost because one has too much energy and the other one has to little energy. This loss of electrons due to Touschek effect reduces the beam lifetime, τ, whose value at ALBA is around 20h in current conditions (see Table I).

The PSF of the pinhole system in FE34 can be experimentally calculated using the Touschek lifetime, T_l. For the ultrarelativistic case, and in ALBA conditions, we have

$$\frac{1}{T_l} \approx \left\langle \frac{cr_p^2 N_p}{2\sqrt{\pi}\gamma^2\sigma_s\sigma_x\sigma_y\delta_m^2} \right\rangle = \left\langle \frac{cr_p^2 I T_{rev}}{2ne\sqrt{\pi}\gamma^2\sigma_s\sigma_x\sigma_y\delta_m^2} \right\rangle \tag{8}$$

where c is the speed of light, r_p is the classical particle radius, N_p is the number of electrons in the bunch, σ_s is the bunch length and δ_m is the relative momentum spread. The beam intensity is $I = nN_p\frac{e}{T_{rev}}$, where n is the number of filled bunches and T_{rev} is the time the electrons take to go a full turn. The brackets mean the average over the whole storage ring circumference. From Eq. (8) we obtain that Touschek lifetime, T_l is directly proportional to the vertical beam size, σ_y, assuming all other parameters remain constant. However, the intensity, I, may slightly vary during the experiment. Then, Touschek lifetime is directly proportional to $\frac{\sigma_y}{I}$.

For normal operating conditions, ALBA lifetime is Touschek dominated for a beam intensity of 100 mA (or more) and $n \sim 400$ bunches. Then, electron losses are mainly produced by Touschek effect and $\tau \approx T_l$, and so,

$$\sigma_y = k \cdot I \cdot \tau, \tag{9}$$

where k is a scaling factor.

Substituting Eq. (9) into Eq. (6) we obtain,

$$\left(\frac{\sigma_{YAG}}{X}\right)^2 = (kI\tau)^2 + \left(\frac{\sigma_{PSF}}{X}\right)^2. \tag{10}$$

During the experiment, we reduce σ_y from 26 μm to 16 μm in 5 steps and we measure the values obtained for I, τ and σ_{YAG} (σ_x remains unchanged). The dataset is shown in Fig. 6 for a Cu filter of 0.3 mm thick in FE34. From the fit values, we find $\sigma_{PSF} = 12 \pm 8$ μm. The large error bar stems from the fact that we cannot reduce further the beam size σ_y. Smaller values of σ_y would provide more data points near the ordinate axis (in Fig.6) and, consequently, the fit uncertainty values would reduce.

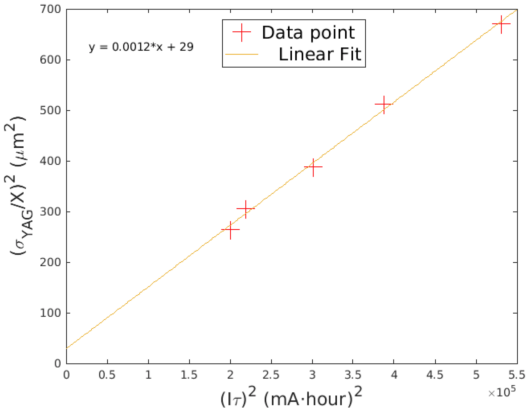

Figure 6: Measurement of σ_{YAG}^2/X^2 versus $(I\tau)^2$, during the experiment.

IV. HEAT LOAD AT THE *AL* WINDOW

In this section we compute the heat load received by Al window according to the analytical Equations found in the literature [7]. In the following we consider a beam intensity of 400 mA, which represents the worst case scenario.

At ALBA, the vertically integrated power emitted per horizontal mrad due to the synchrotron radiation is

$$P[kW] = \frac{26.6}{2\pi}E^3[GeV]B[T]I[A] = 64.93\frac{W}{\text{mrad}}, \tag{11}$$

because radiation is homogeneously emitted in the horizontal plane around the ring. The vertical distribution of the power in units of [W/mrad^2] follows:

$$\frac{dP}{dx'dy'} = \frac{5.42E^4[GeV]B[T]I[A]}{(1+\gamma^2y'^2)^{5/2}}[1+\frac{5\gamma^2y'^2}{7(1+\gamma^2y'^2)}] \tag{12}$$

where (x', y') are the (hor, ver) angles. The profile is shown in Fig. 7, where is also shown that it can be approximated by a Gaussian profile with a standard deviation of

$$\sigma = \frac{0.608}{\gamma} = 0.1 \text{ mrad}. \tag{13}$$

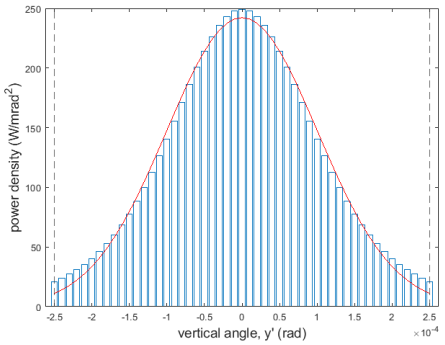

Figure 7: Histogram of the power distribution as a function of the vertical angle y'. The red line is a Gaussian fit assuming σ calculated by Eq. (13). The dotted lines mark the aperture (0.5 mrad) and we see that almost all the radiation and power density goes through the aperture.

Computing the area of the histogram between the vertical apertures of the ALBA pinholes (from ±0.25 mrad), we obtain a total power of 61.16 W per hor mrad, while the area under the Gaussian curve is 61.09 W per hor mrad. The error is about 0.1%, which shows it is a good approximation.

The Aluminium window is placed perpendicularly to the photon beam of 0.5 mrad divergence. The photon flux produced by a dipole after traversing the Al window is obtained with OASYS (see Fig. 3). Knowing that $P = E_{\rm ph} \cdot N_{\rm ph}$, we calculate the power ratio as

$$\frac{P_{\rm Al}}{P_{\rm vac}} = \frac{\int_0^\infty E_{\rm ph} N_{\rm ph}^{\rm Al}\, dE\, |_{\rm Al}}{\int_0^\infty E_{\rm ph} N_{\rm ph}^{\rm vac}\, dE\, |_{\rm vac}} \qquad (14)$$

If we consider P^0 as the power arriving to the Al window, the power transmitted through it is:

$$P_{\rm trans} = P^0 \cdot \frac{P_{\rm Al}}{P_{\rm vac}}, \qquad (15)$$

and the absorbed power is $P_{\rm abs} = P^0$ - $P_{\rm trans}$.

Table V shows the results of these calculations for both FE21 and FE34. The result for FE21 is used by the ALBA Engineering Division to design the cooling system of the Al window.

	FE34	FE21
$P_{\rm trans}$ (W)	20.73	16.61
$P_{\rm abs}$ (W)	40.37	44.49

Table V: Power absorbed and transmitted at the Al windows for both FE21 and FE34.

V. CONCLUSIONS

This work characterizes the pinhole existing at the ALBA FE34 and the new one, still in design stage in FE21. Analytical PSF determination of the FE34 pinhole was already done in 2011. This report compares this result with the one from SRW simulations, and also computes the PSF at FE21 both analytically and with simulations.

With both analytical and simulation methods we obtain that pinhole FE21 resolution is better than the one of pinhole FE34 because of the larger magnification. For the same Cu thickness of 0.3mm, the ultimate pinhole resolutions are ~ 6.6 μm (FE34) and ~ 5 μm (FE21).

For each pinhole the results of $\sigma_{\rm PSF}$ obtained by the different methods are consistent. In FE34, the PSF is also inferred using experimental method, finding a consistent result although the error bar is large.

The electron beam images acquired with SHADOW simulations of the new pinhole in FE21 are useful for predicting the image we will obtain once the new pinhole is constructed. Moreover, the results of $\sigma_{\rm PSF}$ for the pinhole FE21, will be used in the future to calculate the transverse electron beam size.

Finally, the heat load distribution in the Al window in FE21 is given to the ALBA Engineering Division to design the appropriate water cooling system.

Acknowledgments

I would like to thank my supervisors Antoni García-Santiago and Ubaldo Iriso for their advice and encouragement during this project. I would also like to express my appreciation to Andriy Nosych and Dominique Heinis for the help and suggestions in OASYS simulations.

[1] A. Wu Chao, M. Tigner, *Handbook of Accelerator Physics and Engineering*. World Scientific. 1998.

[2] V. Suller, *An X-ray Pinhole Camera Design for the ALBA Synchrotron Light Source*, April 2005.

[3] L. Rebuffi, M. Sanchez del Rio, *OASYS (OrAnge SYnchrotron Suite): an open-source graphical environment for x-ray virtual experiments*, Proc. SPIE 10388, 103880S (2017). DOI: 10.1117/12.2274263

[4] U. Iriso. *Beam Size and Emittance Measurements using the ALBA Pinhole*, ALBA Internal Note AAD-SR-DI-PINH-01. June 2011.

[5] P. Elleaume *et al*, *Measuring Beam Sizes and Ultra-Small Electron Emittances Using an X-ray Pinhole Camera.* J. Synchrotron Rad. (1995). 2, 209-214.

[6] A. Piwinski, *The Touschek effect in strong focusing storage rings*, DESY 98-179, 1998, http://arxiv.org/abs/physics/9903034.

[7] J.A. Clark. *The Science and Technology of Undulators and Wigglers*, Ed. Oxford Science Publications, 2004.